PTH Induces Systemically Administered Mesenchymal Stem Cells to Migrate to and Regenerate Spine Injuries

Dmitriy Sheyn,[1,2] Galina Shapiro,[3] Wafa Tawackoli,[1,2,4] Douk Soo Jun,[1] Youngdo Koh,[1] Kyu Bok Kang,[1] Susan Su,[1,2] Xiaoyu Da,[4] Shiran Ben-David,[1,2] Maxim Bez,[3] Eran Yalon,[3] Ben Antebi,[3] Pablo Avalos,[2] Tomer Stern,[5] Elazar Zelzer,[5] Edward M Schwarz,[6,7] Zulma Gazit,[1,2,3] Gadi Pelled,[1,2,3] Hyun M Bae[1] and Dan Gazit[1,2,3,4]

[1]Department of Surgery, Cedars-Sinai Medical Center, Los Angeles, California, USA; [2]Board of Governors Regenerative Medicine Institute, Cedars-Sinai Medical Center, Los Angeles, California, USA; [3]Skeletal Biotech Laboratory, Hebrew University of Jerusalem, Jerusalem, Israel; [4]Biomedical Imaging Research Institute, Cedars-Sinai Medical Center, Los Angeles, California, USA; [5]Department of Molecular Genetics, Weizmann Institute of Science, Rehovot, Israel; [6]The Center for Musculoskeletal Research, University of Rochester Medical Center, Rochester, New York, USA; [7]Department of Orthopedics, University of Rochester Medical Center, Rochester, New York, USA

Osteoporosis affects more than 200 million people worldwide leading to more than 2 million fractures in the United States alone. Unfortunately, surgical treatment is limited in patients with low bone mass. Parathyroid hormone (PTH) was shown to induce fracture repair in animals by activating mesenchymal stem cells (MSCs). However, it would be less effective in patients with fewer and/or dysfunctional MSCs due to aging and comorbidities. To address this, we evaluated the efficacy of combination i.v. MSC and PTH therapy versus monotherapy and untreated controls, in a rat model of osteoporotic vertebral bone defects. The results demonstrated that combination therapy significantly increased new bone formation versus monotherapies and no treatment by 2 weeks ($P < 0.05$). Mechanistically, we found that PTH significantly enhanced MSC migration to the lumbar region, where the MSCs differentiated into bone-forming cells. Finally, we used allogeneic porcine MSCs and observed similar findings in a clinically relevant minipig model of vertebral defects. Collectively, these results demonstrate that in addition to its anabolic effects, PTH functions as an adjuvant to i.v. MSC therapy by enhancing migration to heal bone loss. This systemic approach could be attractive for various fragility fractures, especially using allogeneic cells that do not require invasive tissue harvest.

Received 8 May 2015; accepted 13 November 2015; advance online publication 9 February 2016. doi:10.1038/mt.2015.211

INTRODUCTION

Osteoporosis is a chronic and life-threatening disease affecting more than 200 million people worldwide.[1,2] Osteoporosis often remains asymptomatic until a fracture occurs. Its pathogenesis stems from an improper balance between bone formation and bone resorption, resulting in low bone mass, impaired bone architecture, and increased risk of fractures.[3] Current osteoporosis treatments consist of lifestyle measures recommended for all patients and pharmacologic therapy reserved for high fracture risk patients. Antiresorptive oral bisphosphonates are recommended to most patients as the first-line pharmacologic therapy in spite of their inability to restore lost bone mass. Second-line therapies include denosumab the fully human monoclonal antibody to the receptor activator of nuclear factor kappaB ligand (RANKL) and the anabolic 1–34 portion of recombinant human parathyroid hormone (PTH, teriparatide). While these preventive pharmacotherapies reduce the risk of vertebral (30–70%) and nonvertebral fractures (12–53%), depending on agents and patients' compliance, none of these agents are indicated for fracture healing.[4]

The most common fragility fractures are osteoporosis-related vertebral compression fractures (OVCFs) (>750,000 fractures/year in the United States), which are associated with significantly high morbidity and mortality rates.[5] As many as 150,000 OVCFs require hospitalization annually, which usually involves prolonged bed rest and i.v. administration of analgesic agents, which may worsen the underlying osteoporosis. When fractures occur, surgery is usually not an option for patients with osteoporosis due to the low bone density of their vertebral bodies. Unfortunately, neither is the previously advocated[6,7] minimally invasive percutaneous injection of polymethylmethacrylate into the affected vertebral body, which was later proven as no more effective than sham surgery in randomized clinical trials.[8,9] Therefore, there is a clear medical need for the development of new, noninvasive therapies to treat OVCFs.

Mesenchymal stem cells (MSCs) can differentiate into osteoblasts, chondrocytes, and adipocytes.[10,11] Systemically administered MSCs migrate preferentially to injury sites in various

The first two authors contributed equally to this work.
The last three authors should be considered as equal senior authors.
Correspondence: *Dan Gazit, Skeletal Regeneration and Stem Cell Therapy Program, Molecular & Micro Imaging Core, Department of Surgery, The Board of Governors Regenerative Medicine Institute (RMI), Cedars-Sinai Medical Center, AHSP, Rm A8108, 8700 Beverly Blvd., Los Angeles, California 90048, USA. E-mail: dan.gazit@csmc.edu*

disease models.[4] Although the exact mechanism for this activity is not fully understood, it is likely that the injured tissue secretes specific ligands that facilitate migration, adhesion, and infiltration of MSCs, similar to the mechanism seen in recruitment of leukocytes to sites of inflammation. MSCs can be reintroduced into the donor as an autologous graft or used as allogeneic cells to treat other recipients. Unfortunately, autologous MSCs may not be a suitable treatment for OVCFs, because patients with osteoporosis have fewer MSCs or MSCs that are less prone to proliferate and differentiate into osteoblasts and consequently form bone.[6,7] Since allogeneic MSCs do not require a cell isolation phase for each patient and are believed to be immunomodulatory, their use is considered advantageous for the clinical setting. Indeed, allogeneic MSCs are being evaluated in many clinical trials as a systemic therapy for various diseases.[6]

To achieve efficient tissue regeneration following systemic administration of stem cells, a sufficient supply of cells must migrate to the injury site and subsequently differentiate *in situ*. In addition to being US Food and Drug Administration (FDA) approved for fragility fracture prevention, PTH has been shown in preclinical studies to increase endogenous MSC migration to injury sites,[12] promote osteoblast progenitor proliferation and differentiation,[13,14] and decrease osteoblast apoptosis. However, these preclinical studies not only used extremely high PTH dosages, ~140 times the clinical dosage, but also did not increase the number of available functional MSCs thereby limiting the potential efficacy of PTH.

Here, we hypothesized that combining systemic injection of exogenous MSCs and daily intermittent administration of PTH would enhance MSC migration to vertebral fractures, leading to osteogenic differentiation and eventual fracture repair in osteoporotic animals. We further speculated that combined MSCs–PTH therapy would yield a synergistic effect on bone regeneration that would be superior to either treatment alone.

RESULTS

Osteoporotic rat study

A rat model of postmenopausal osteoporosis was generated in immunocompromised rats that can sustain human cell implantation by ovariectomy in conjunction with a low-calcium diet (LCD); a similar model was previously reported using immunocompetent rats.[2] Once ovariectomy and 4 months of LCD were found to be sufficient to induce osteoporosis (**Supplementary Figure S1**), a different group of rats underwent this induction protocol and were subsequently switched to a regular diet (post-LCD). Micro-computed tomography (μCT) was used to scan these rats before initiation of the LCD and again on day 0 and at weeks 8 and 12 post-LCD to verify the persistence of osteoporosis with little spontaneous bone mass augmentation (**Figure 1c–e**). Hematoxylin and eosin staining further validated the drastic reduction in the trabecular bone component in the animals' lumbar vertebrae following a 4-month LCD (**Figure 1f**). Consequently, a 4-month LCD was deemed optimal to achieve maximal irreversible osteoporosis and was used throughout the study.

MSC migration to vertebral bone defects

Human MSCs (hMSCs) were infected with a lentiviral vector harboring the reporter gene *luciferase2* (*Luc2*) under the constitutive ubiquitin promoter to allow *in vivo* imaging of migration activity. Stable transfection of hMSCs-Luc2 and constitutive expression of *Luc2* were validated by performing quantitative bioluminescence imaging (BLI) over six passages (**Figure 2a,b**). No significant change ($P > 0.05$) in *Luc2* expression was found in subsequent passages, indicating that BLI could be used to track hMSCs-Luc2 *in vivo*.

Cylindrical defects were created in two lumbar vertebral bodies in each osteoporotic rat. The rat then received a total of five i.v. injections of saline or hMSCs-Luc2 and phosphate-buffered saline (PBS), low-dosage PTH (ldPTH), or hdPTH daily starting on postoperative day 3 (**Figure 1a**). The rats were monitored using BLI for 56 days postoperatively. At each time point the bioluminescent signal overlaying the lumbar region was quantified (**Figure 2c**). Next, a cumulative sum of bioluminescent signals (Σ total flux) was plotted against time for the different treatment groups (**Figure 2d**). The results showed an increase in Σ total flux ($r^2 = 0.92$) for the hMSCs-Luc2 group during the 56 days of the study, indicating that hMSCs in this group both migrated to and engrafted in the lumbar region. A significantly higher Σ total flux was found for rats treated with hMSCs-Luc2+hdPTH as early as 7 days postoperatively ($P \leq 0.05$) and for all subsequent time points ($P \leq 0.01$), but not for rats treated with hMSCs-Luc2+ldPTH. Overall, the trend of accumulation of MSCs in animals treated with MSCs-Luc2+hdPTH was logarithmic ($r^2 = 0.98$), whereas in animals not treated with PTH it was linear, indicating profound changes in the pattern of MSC recruitment to the fracture site and in the cells' subsequent survival.

The effect of hMSC-PTH treatment on vertebral bone defect regeneration

The therapeutic effect of combined IV-MSC and PTH therapy was evaluated using ldPTH and hdPTH (**Supplementary Figure S4**). The effect was then compared to each monotherapy, and to that of no treatment (hereafter referred as "control"). Bone regeneration in vertebral defects was monitored at several time points after surgery by performing *in vivo* μCT (**Figure 3a**). By analyzing the scans, we were able to quantify bone volume density (BVD; **Figure 3b**), an indication of bone formation, and apparent density (AD; **Figure 3c**), calculated as the mean mineral density of the segmented bone. The results indicated minimal bone regeneration during the first 2 weeks postoperatively, and no additional bone formation at later time points in the control and hMSCs groups (**Figure 3a–c**). New bone formed mostly at the edges of the defect (**Figure 3a**). No significant differences in either BVD or AD were found between the two groups ($P > 0.05$) at any time point. Significantly enhanced bone formation was not found in rats treated with ldPTH, compared with the control groups ($P > 0.05$; **Figure 3b**). Only in rats treated with hMSCs+ldPTH was increased formation of cortical and trabecular bone evident on both 2D tomographic images and 3D reconstructed images as soon as week 2 postoperatively (**Figure 3a**). At this time point, significantly higher BVD ($P \leq 0.05$; **Figure 3b**) and AD ($P \leq 0.01$; **Figure 3c**) values were found in the hMSCs+ldPTH group than in the control and single-treatment groups. Both hMSCs+PTH treatments were superior to all other treatments except hdPTH alone, in BVD at 4 weeks postoperatively ($P \leq 0.01$; **Figure 3b**).

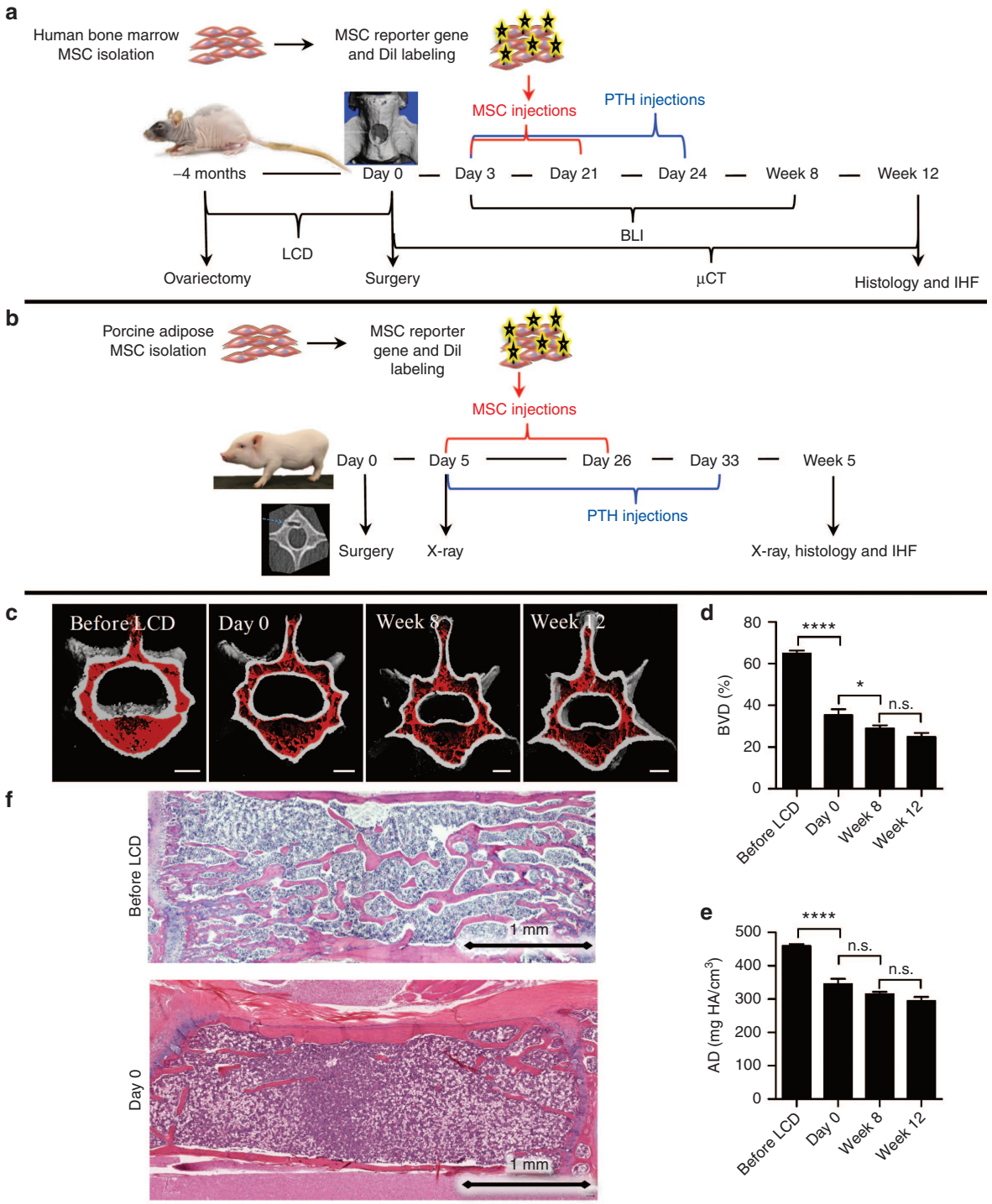

Figure 1 Experimental design and model establishment. (**a**) Human bone-marrow mesenchymal stem cells (MSCs) were isolated, labeled to express the reporter gene *Luciferase*, and stained with DiI. Multiple vertebral defects were created in ovariectomized athymic rats after 4 months of low-calcium diet (LCD). These rats were daily administered parathyroid hormone (PTH) or PBS and given five i.v. injections of human bone-marrow MSCs or saline. Cell migration to vertebral defects was tracked using bioluminescence imaging (BLI), and bone regeneration was analyzed using µCT. Twelve weeks postoperatively, the vertebrae were harvested for histology and immunofluorescence. (**b**) Multiple lumbar vertebral defects were created in minipigs. The minipigs were administered PTH or vehicle and given four i.v. injections of porcine adipose MSCs or saline. Bone regeneration was monitored using x-ray fluoroscopy and µCT. Five weeks postoperatively, the vertebrae were harvested for histology and immunofluorescence. (**c**) Bone loss induced by ovariectomy and LCD in athymic rats' lumbar vertebrae was evaluated using longitudinal *in vivo* µCT. The trabecular component is highlighted in red. (**d**,**e**) The trabecular component was then quantitatively compared over time for changes in bone volume density (BVD) and apparent density (AD). Data are shown as mean + SEM ($n = 5$). Repeated-measures one-way ANOVA with bonferroni correction for multiple comparisons was preformed; n.s., not significant; *$P < 0.05$, and ****$P < 0.0001$. (**f**) Osteopenia was assessed using H&E-stained histological sections of the lumbar vertebrae. H&E, hematoxylin and eosin.

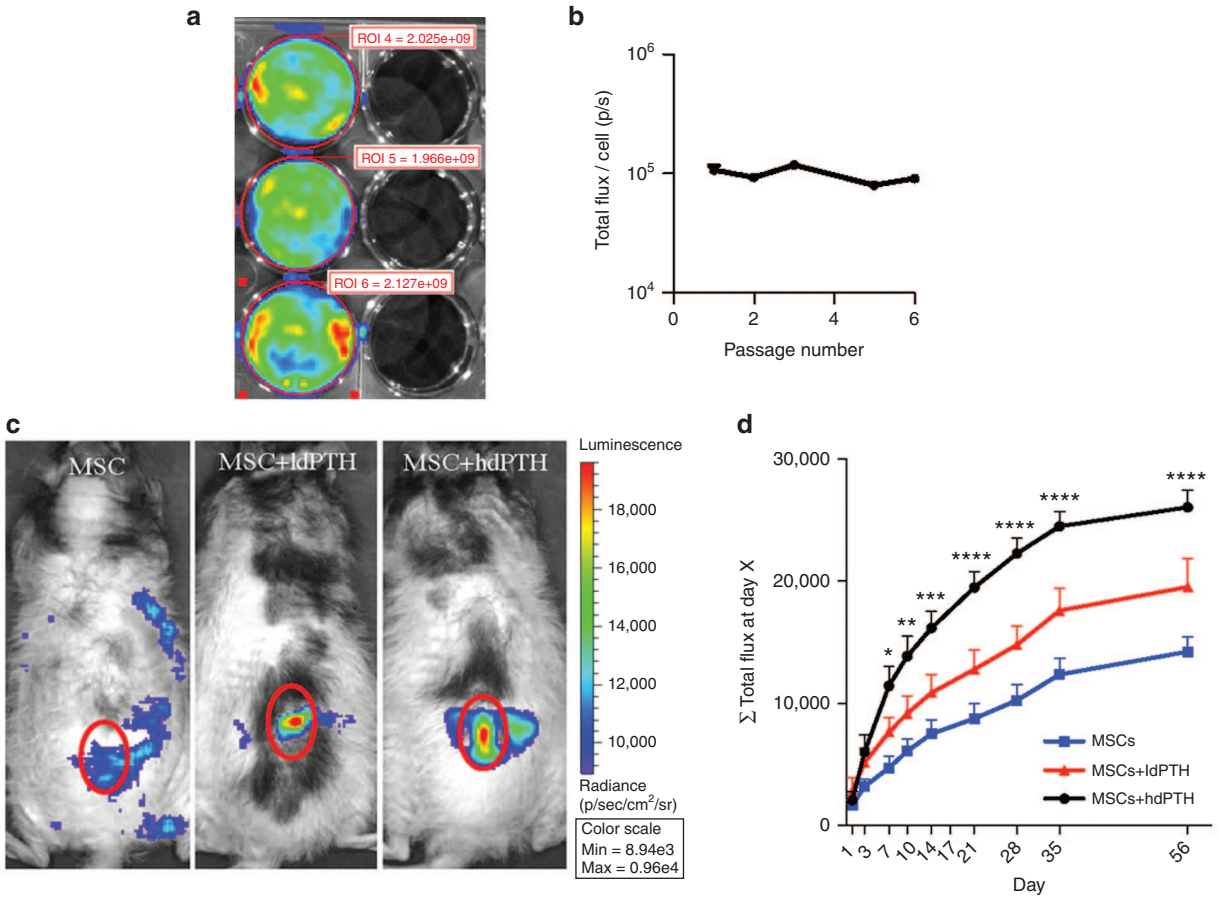

Figure 2 Parathyroid hormone enhances mesenchymal stem cell migration to vertebral defects. (**a**) Human mesenchymal stem cells (hMSCs) were transduced with the lentiviral vector harboring the reporter gene *Luciferase2* (hMSC-Luc2). Representative *in vitro* bioluminescence imaging (BLI) of three confluent hMSC-Luc2 seeded wells (left) compared to three background wells without cells (right) is shown. (**b**) *Luciferase2* expression was quantified based on *in vitro* BLI over six passages. Data are shown as mean + SEM ($n = 5$). One-way ANOVA with Bonferroni correction for multiple comparisons was preformed; n.s., not significant. (**c**) hMSC-Luc2 migration to vertebral defects was tracked over 8 weeks after the first cell injection and quantified by measuring the bioluminescent signal overlying the vertebral defects. Representative images of all three groups treated with hMSC-Luc2 (without PTH, ldPTH, and hdPTH) taken on postoperative day 14 are presented along the scale of the total flux. The red circle on the representative images indicates the region of interest in the lumbar spine proximity that was analyzed. (**d**) The average cumulative total flux (Σ total flux) up to each time point was calculated per animal. Data are shown as mean + SEM ($n = 5$ for each group). Repeated-measures two-way ANOVA with bonferroni correction for multiple comparisons was preformed. *$P < 0.05$; **$P < 0.01$; ***$P < 0.001$; and ****$P < 0.0001$.

Interestingly, while neither BVD nor AD appear to change between weeks 2 and 4 postoperatively in hMSCs+ldPTH treated rats, the distribution of the newly formed bone appears to shift from a trabecular component to a cortical component. This might be related to accelerated remodeling of trabecular bone in comparison to cortical bone due to increased blood supply but could also could be an outcome of a therapeutic approach based on increased stem cell fracture tropism. By week 8, bone formation in the hMSCs+ldPTH group was sufficient to regenerate the cortex completely, whereas in rats, in the control groups, there was clearly cortical discontinuity and lower bone mass (**Figure 3a**). Interestingly, while no significant difference in BVD was found between the hMSCs+hdPTH group and the hdPTH group at any time point ($P > 0.05$; **Figure 3b**), a significant difference in AD was found at week 8 between these two groups ($P \leq 0.01$; **Figure 3c**). Therefore, while PTH was administered for a short period, a significant lasting positive effect on AD was found only when PTH was combined with MSCs. Histological analysis showed that there was too little regrowth to regenerate cortex or trabeculae in the control and MSCs groups (**Figure 4a**). In ldPTH-treated animals, the defect was partially regenerated, but only in hMSCs+ldPTH–treated animals (**Figure 4a**) were both cortex and trabeculae regenerated. Similar trends were found for the hdPTH and hMSCs+hdPTH groups (**Supplementary Figure S2A**).

Fate of i.v.-injected hMSCs

To investigate the contribution of systemically administered MSCs to vertebral defect regeneration, we labeled these cells with 1,1'-dioctadecyl-3,3,3',3'-tetramethylindocarbocyanine perchlorate (DiI) before injection and later stained retrieved tissue sections with immunofluorescent antibodies against the osteogenic markers bone sialoprotein and osteocalcin. Although we used antibodies against human osteogenic markers, some cross-reactivity with rat proteins was expected, and thus not all osteogenic cells co-localized with the DiI-stained donor human cells (**Figure 4b**), indicating contribution of host

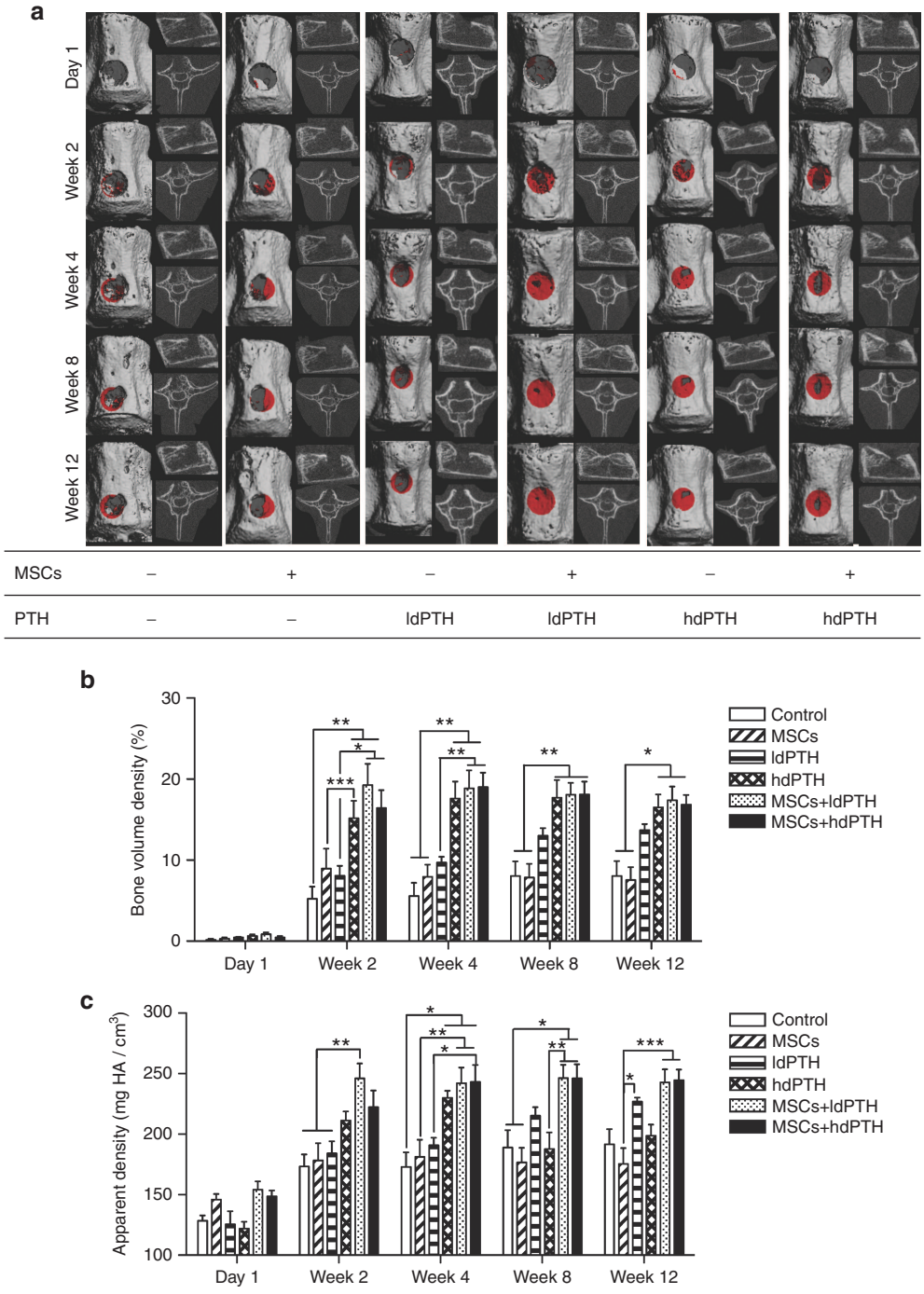

Figure 3 Intravenous mesenchymal stem cells and parathyroid hormone combination therapy regenerates vertebral defects in osteoporotic rats: micro-computerized tomography analysis. (**a**) Rats with identical vertebral bone voids were treated with mesenchymal stem cells (MSCs) or saline and with low-dosage parathyroid hormone (ldPTH), high-dosage parathyroid hormone (hdPTH), or vehicle. The animals were imaged using micro-computed tomography 1 day and 2, 4, 8, and 12 weeks postoperatively. A representative vertebral defect at various time points for each group is depicted in each panel as a frontal 3D image (left side) with new bone formation in the void highlighted in red, a sagittal 2D image (upper right), and an axial 2D image (lower right). (**b** and **c**) Quantitative analysis of bone formation in the voids was performed and bone volume density and apparent density were calculated. Data are shown as mean + SEM (control: $n = 7$; MSCs: $n = 9$; ldPTH: $n = 8$; hdPTH: $n = 9$; MSCs+ldPTH: $n = 8$; MSCs+hdPTH: $n = 9$). Repeated measures two-way ANOVA with Bonferroni correction for multiple comparisons was preformed; $^{*}P < 0.05$, $^{**}P < 0.01$, and $^{***}P < 0.001$.

cells. The DiI-stained cells were found in vertebral defects in all MSCs-injected groups; however, the abundance of cells appeared qualitatively higher in animals that were also treated with PTH. Many injected cells were found in cancellous bone, where new tissue formed, but not in the cortical region. Co-localization of DiI-stained cells and osteocalcin and bone sialoprotein showed that some of the injected cells expressed either or both differentiation markers, while others expressed

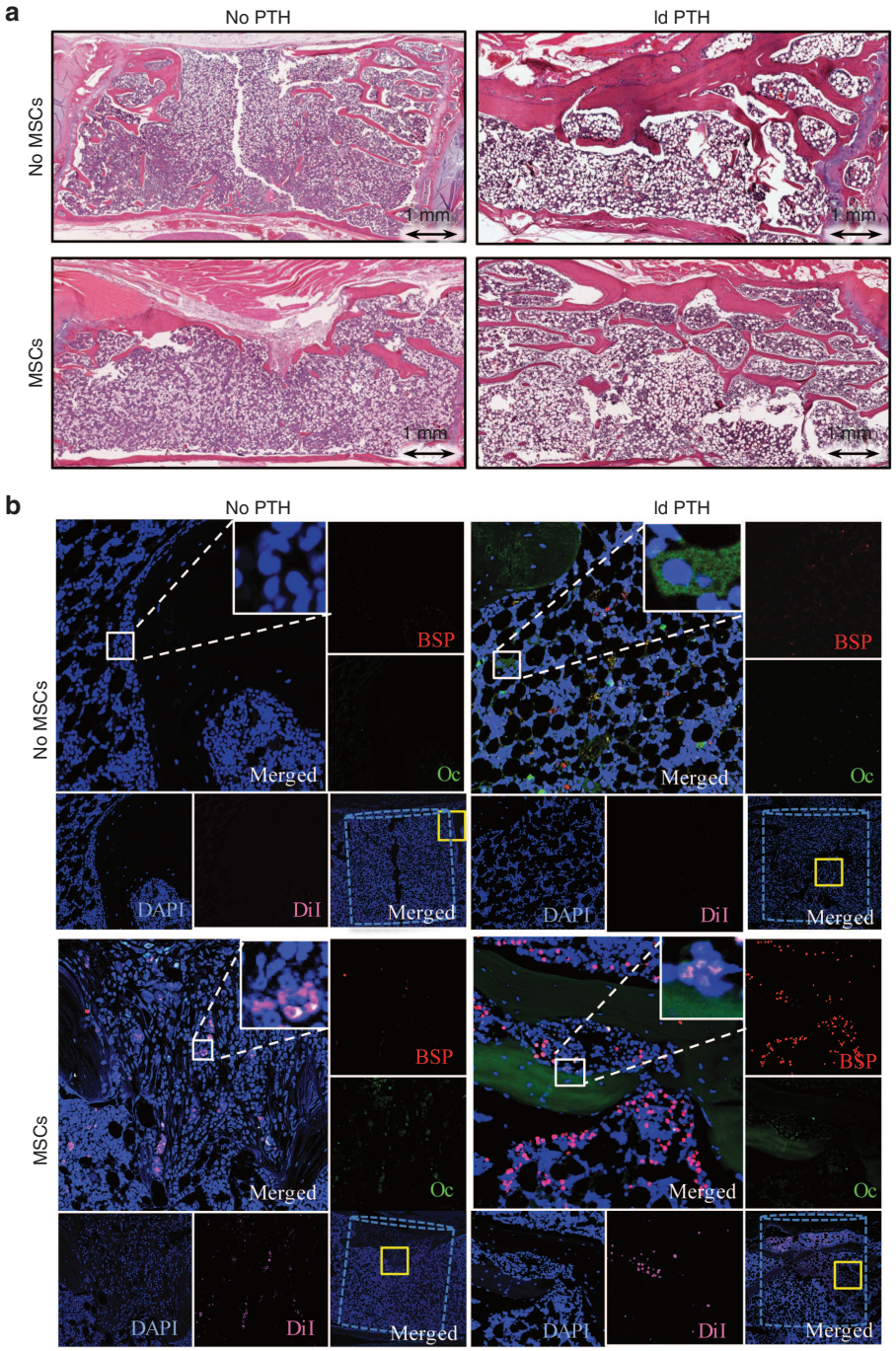

Figure 4 Intravenous mesenchymal stem cells and parathyroid hormone therapy regenerates vertebral defects in osteoporotic rats: histological and immunofluorescence analyses. (**a**) Representative vertebral defects of animals that received low-dosage PTH (ldPTH) or vehicle and DiI-labeled mesenchymal stem cells (MSCs) or saline were harvested, decalcified, embedded in paraffin and sectioned. Slides were stained with standard hematoxylin and eosin and imaged with light microscopy. (**b**) Serial slides were also immunostained against the osteogenic markers osteocalcin (Oc), bone sialoprotein (BSP), and counterstained with DAPI. Slides were imaged using confocal microscopy for DAPI, DiI-labeled MSCs, Oc, and BSP. A representative panel for each treatment group includes: (**i**) a merged image of the defect site with the bone void marked by a dashed cylinder and an area subsequently magnified marked by a solid yellow square (bottom right corner); (**ii**) a merged magnification of the area denoted by the yellow square (top left corner) with a built in magnification of the solid white square in its' top right corner; (**iii**) four single channel magnifications of the solid yellow square-marked area along the right and bottom edges denoted: BSP, Oc, DAPI, and DiI corresponding to the stain in the subfigure. DAPI, 4',6-diamidino-2-phenylindole dihydrochloride.

neither. Some staining for osteogenic markers was observed in the PTH-treated groups; this was probably due to the anabolic effects of PTH. Importantly, more MSCs were visible in the regenerated defects of i.v.-MSC and PTH-treated rats. In addition to the microscopic detection of MSCs in the defect area, the systemic biodistribution of these cells was evaluated using PCR against *Luc2*. Evidence of MSCs was found only in the animals' lungs (**Supplementary Figure S2**).

Expression of cell migration and chemoattraction molecules

To look into the mechanism of PTH-induced stem cell migration to vertebral defects, we assessed the activation of two previously investigated pathways of cell migration. First, we investigated the most extensively studied pathway of stem cell mobilization and migration to injury sites, the stromal cell-derived factor 1 (SDF1)/C-X-C chemokine type 4 (CXCR4) axis, which is known to be enhanced by PTH therapy.[15,16] In this study, we stained harvested vertebrae sections to determine the expression of SDF1 by host cells in the defect site and that of CXCR4, a receptor for SDF1, which reportedly is expressed by migrating cells.[15] We found SDF1-expressing cells in the vertebral defects of PTH-treated animals that had been treated with or without hMSCs, but no SDF1 expression in the control group. As for CXCR4, we detected a few positive cells in tissue from animals in the hMSCs-treated group, some of which could be co-localized with DiI-labeled donor cells (**Figure 5a**). In the i.v.-MSC and PTH-treated group, we found abundant DiI-labeled MSCs co-expressing CXCR4, while SDF1 expression was limited to host cells within and at the margins of the defect. We found no CXCR4 expression in the PTH-treated groups. Zhu *et al.*[17] found that PTH also attracts MSCs to injury sites by stimulating expression of amphiregulin, an epidermal growth factor–like ligand that signals through the epidermal growth factor receptor (EGFR), in both osteoblasts and osteocytes. Here, we stained the vertebral defect sites with antibodies against both the secreted ligand (amphiregulin) and the receptor (EGFR). Similarly to SDF1/CXCR4 expression, amphiregulin was detected in the PTH groups and EGFR staining was colocalized with DiI-labeled MSCs (**Figure 5b**).

Minipig study

Following the results of the rat study, we investigated the effect of the combined IV-MSC and PTH treatment on vertebral bone regeneration in an immunocompetent large animal model. Bone defects were created in the lumbar vertebrae of minipigs (**Figure 1b**), similarly to what was previously reported.[8,9] The minipigs were treated with either four i.v. injections of allogeneic porcine MSCs (pMSCs) or PBS once a week and with daily s.c. injections of PBS or 1.75 µg/kg PTH for 4 weeks. Bone formation was monitored using *in vivo* x-ray fluoroscopy followed by *ex vivo* µCT scanning. We analyzed nine defects for each group (three pigs with three defects each).

Bone regeneration in minipig vertebral defects

Lateral x-ray films obtained few days postoperatively showed radiolucent defects that were similar in size and anatomical location (**Figure 6a**). On postoperative week 5, these defects remained clearly visible in all control groups but not in the pMSCs+PTH group. In the control groups, a radiopaque rim indicated bone formation at the circumference of the defect site, but the defects themselves did not appear to have healed because they remained more radiolucent than the tissue around them. In contrast, in minipigs treated with pMSCs+PTH, the defect sites themselves were more radiopaque than surrounding uncompromised tissue, indicating that the previously missing bone had regenerated at a greater mineral density than native vertebral bone. The

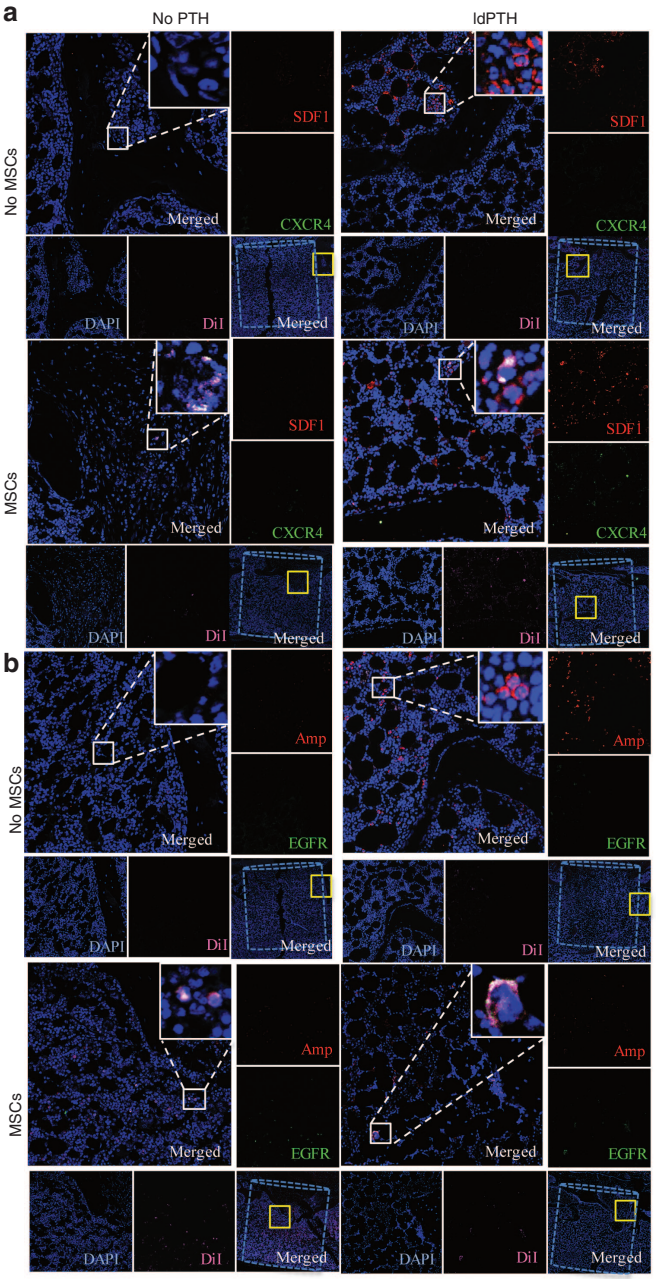

Figure 5 Parathyroid hormone enhances migration of mesenchymal stem cells to the defect site via two pathways: confocal imaging of immunofluorescent staining. Representative vertebral defects of animals that received low-dosage PTH (ldPTH) or vehicle and DiI-labeled mesenchymal stem cells (MSCs) or saline were harvested, decalcified, embedded in paraffin, and sectioned. Slides were immunostained against migration markers (**a**) stromal cell-derived factor 1 (SDF1) and C-X-C chemokine type 4 (CXCR4) or (**b**) epidermal growth factor receptor (EGFR) and amphiregulin (Amp) and both sets counterstained with DAPI. Slides were imaged using confocal microscopy and a representative panel for each treatment group is shown including: (i) a merged image of the defect site with the bone void marked by a dashed cylinder and an area subsequently magnified marked by a solid yellow square (bottom right corner); (ii) a merged magnification of the area denoted by the yellow square (top left corner) with a built in magnification of the solid white square in its' top right corner; (iii) four single channel magnifications of the solid yellow square-marked area along the right and bottom edges named corresponding to the stain in the subfigure. DAPI, 4',6-diamidino-2-phenylindole dihydrochloride.

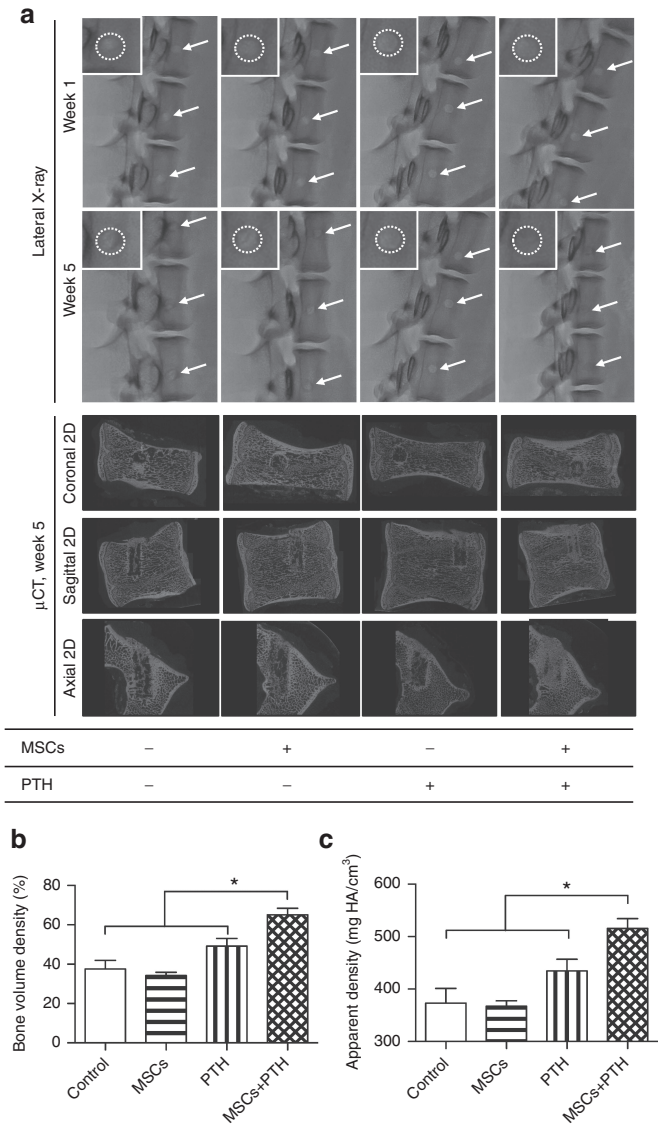

Figure 6 Intravenous mesenchymal stem cells and parathyroid hormone therapy regenerates minipig vertebral defects: *in vivo* x-ray and micro-computerized tomography imaging. (**a**) Vertebral bone voids treated with mesenchymal stem cells (MSCs) or saline and with parathyroid hormone (PTH) or PBS were imaged *in vivo* using x-ray fluoroscopy on weeks 1 and 5 postoperatively and *ex vivo* using micro-computerized tomography (μCT). Representative lateral radiographs of L2–4 for each group are shown with white arrows pointing at the voids. A magnification of one of these voids with a white dashed circle marking the void circumference is shown in the upper left corner of each radiograph. Representative coronal, sagittal, and axial 2D μCT images are also shown for each group. (**b** and **c**) A μCT-based quantitative analysis of bone formation in the voids was performed, and bone volume density and apparent density were calculated. Data are shown as mean + SEM (control: $n = 6$; MSCs: $n = 5$; PTH: $n = 8$; MSCs+PTH: $n = 9$). Two-way ANOVA with bonferroni correction for multiple comparisons was preformed; $^*P < 0.05$.

x-ray findings were corroborated by a μCT analysis, which indicated that the BVDs ($P \leq 0.05$; Figure 6b) and ADs ($P \leq 0.05$; Figure 6c) of defect sites treated with pMSCs+PTH were about two times higher than those measured in controls. In conclusion, only minipigs treated with both pMSCs+PTH showed complete healing of the bone defect, while neither treatment alone seemed to affect the healing process ($P > 0.05$; Figure 6b,c). Histological analysis showed that, in the control groups, there was cortex-like formation of dense bone at the edges of the defect, whereas in the i.v.-MSC and PTH-treated group, the defect site was filled with trabecular bone that was denser than surrounding uncompromised vertebral bone (Figure 7a).

Fate of i.v.-injected pMSCs

The contribution of allogeneic porcine MSCs to the regeneration of bone defects was detected using fluorescence microscopy and imaging of the i.v.-injected DiI-labeled cells (Figure 7b,c). Similarly to the rat model, administered cells were found mostly in the region of the defect, in the bone marrow of newly formed bone tissue and not incorporated in the trabecular bone tissue itself. Also, similarly to the rats, some of the cells were co-localized with osteocalcin-expressing cells, indicating osteogenic differentiation. In addition to MSCs found at the defect site, other MSCs were detected in the spleen and liver, but not in pigs treated with pMSCs+PTH (**Supplementary Figure S3**).

DISCUSSION

Our results showed that vertebral defects created in osteoporotic rats and in healthy pigs were efficiently repaired following combined i.v.-MSCs+PTH treatment. This contrasts with the results in animals that received either treatment alone or no treatment. Moreover, the results support the hypothesis that administration of PTH enhanced hMSC migration to vertebral bone defects in osteoporotic rats.

Current treatment of patients with osteoporosis mostly focuses on OVCF prevention using medicines such as alendronate sodium and PTH.[18] Teriparatide (the 1–34 portion of PTH) is the only FDA-approved osteoporosis anabolic agent. Preclinical studies support the potential for PTH as a treatment for bone fractures. Einhorn and colleagues demonstrated that PTH improves fracture callus quality, increases bone mineral content and density, and accelerates endochondral ossification in a rat femur diaphyseal fracture model.[19] Kaback *et al.*[12] also investigated the mechanisms underlying PTH-accelerated long-bone fracture repair by assessing the phenotype of MSCs from mice treated with 40 μg/kg PTH or saline for 7 days. Their results showed that PTH induced the osteoblast transcription factors Osx and Runx2 in MSCs and accelerated osteoblast maturation and fracture healing in these mice. Other reports demonstrated that PTH stimulates MSC recruitment to bone by inducing CXCL12 and SDF1 expression in osteoblasts.[15]

Although randomized clinical trials have demonstrated that PTH therapy accelerates fracture healing,[20,21] several conflicting results were found. These differences may be related to differences in study design including the fracture site and PTH dosage, and thus more evidence is needed to know if teriparatide alone accelerates fracture repair. In this study, we showed in a rat model of osteoporosis that a clinically relevant dosage of PTH had a limited effect on vertebral bone repair and was significantly inferior to the combined therapy of PTH and MSCs. These results could pave the way for further exploration of the efficacy of PTH and MSC combination therapy in additional fragility fractures and cases of

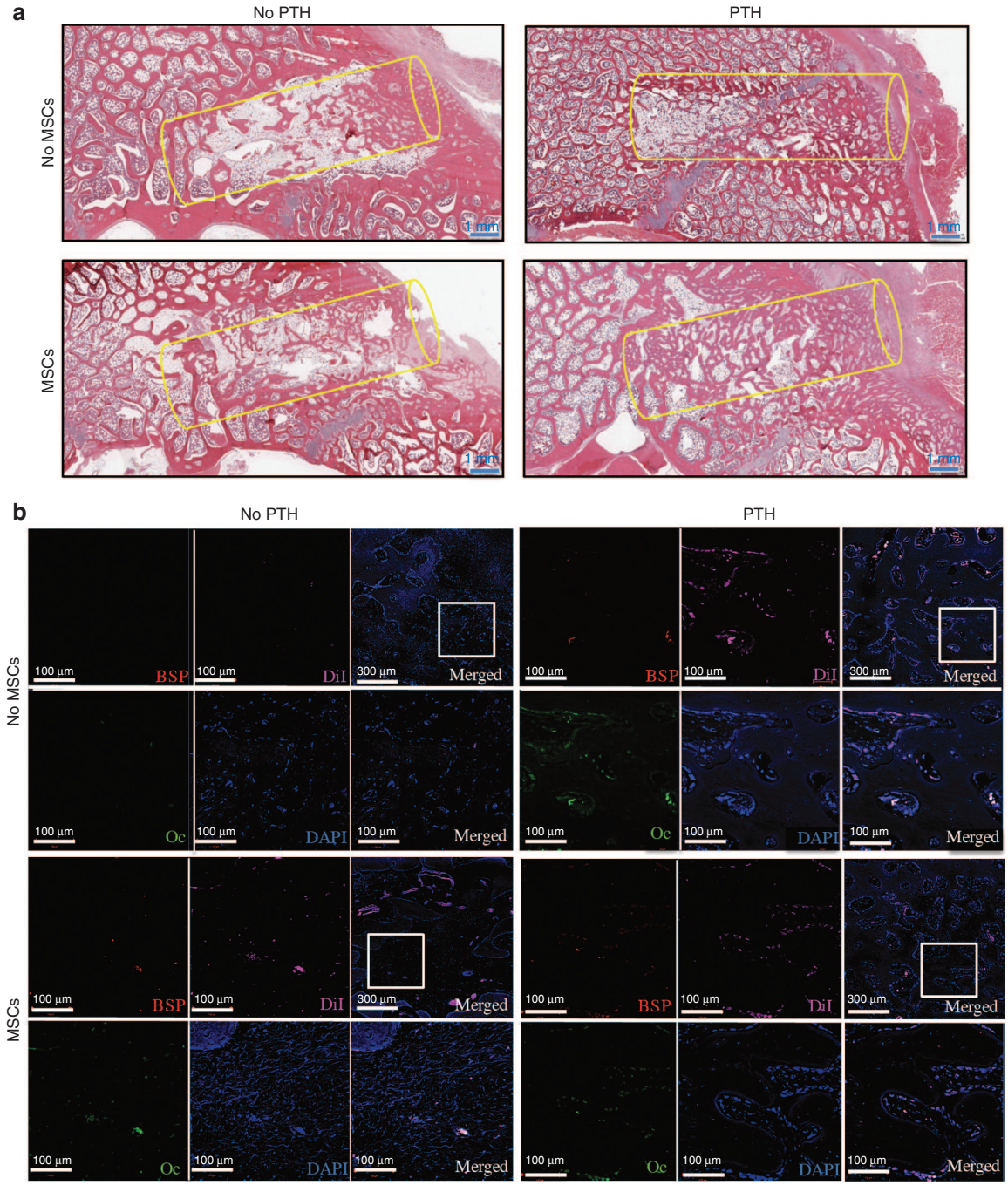

Figure 7 Intravenous mesenchymal stem cells and parathyroid hormone therapy regenerates vertebral defects in minipigs: histological and immunofluorescence analyses. Representative vertebral defects of animals that received PTH or vehicle and DiI-labeled mesenchymal stem cells (MSCs) or saline were harvested, decalcified, embedded in paraffin, and sectioned. (**a**) Slides were stained with standard hematoxylin and eosin and imaged with light microscopy. (**b**) Slides were also immunostained against the osteogenic markers Osteocalcin (Oc), bone sialoprotein (BSP), and counterstained with DAPI. Slides were imaged using confocal microscopy for DAPI, DiI-labeled MSCs, Oc, and BSP. A representative panel for each treatment group includes: (i) a merged image of the defect site with an area subsequently magnified marked by a white square (top right corner); (ii) a merged magnification of the area denoted by the white square (bottom right corner); (iii) four single channel magnifications of the white square-marked area denoted: BSP, Oc, DAPI, and DiI corresponding to the stain in the subfigure. DAPI, 4′,6-diamidino-2-phenylindole dihydrochloride.

bone loss such as hip fractures and craniofacial bone defects. We believe that this novel therapeutic approach has great potential to be successfully applied when allogeneic stem cells are appropriate for bone regeneration.

The anabolic effects of PTH include increases in skeletal mass, bone turnover, and bone strength.[22,23] However, continuous release of excess endogenous PTH, as occurs in hyperparathyroidism, may be detrimental to the skeleton because bone resorption

is stimulated more than bone formation, which limits the duration of safe treatment.[24,25] Therefore, the dosage of PTH and the duration of intermittent administration play a critical role in therapeutic outcome. Currently, the FDA-approved treatment is 20 μg/day (~0.3–0.5 μg/kg) for up to 2 years. The dosage used in preclinical studies to enhance fracture repair is 0.4–40 μg/kg[26,27] in small animals and 1–5 μg/kg in large animals.[28,29] Some studies showed a clear dose response to PTH,[19,28] whereas other studies showed that higher dosages of PTH did not necessarily provide better outcomes.[20,30] In agreement with findings in the latter studies, our results showed that a dosage of 0.4 μg/kg (ldPTH, equivalent to the clinical dosage of 20 μg/day) was more successful in accelerating and maintaining the repair of a bone defect in osteoporotic rats when combined with MSCs. Our results in pigs were achieved using a higher dosage (1.75 μg/kg); however, this is a much lower dosage than those reported in other large animals studies.[26,28]

This study demonstrates effective regeneration of vertebral defects that mimic compression fractures by using noninvasive systemic stem-cell-and-hormone therapy. While others have previously established vertebral bone defects as an injury model in osteoporotic sheep,[31] this is the first study to our knowledge to develop an immunocompromised rat OVCF model based on previously separately published rat osteoporosis[2,32,33] and rat vertebral defect models.[34–36] Combining ovariectomy with a LCD was used to rapidly induce osteoporosis but LCD was not required for modeled osteoporosis maintenance (**Figure 1d**) and therefore rats were switched to a regular diet after 4 months of LCD. This novel rodent model offers a highly reproducible, multiple injuries per animal, readily quantifiable, and versatile system that allowed us to study a human cell therapy for fragility fractures. Nevertheless, it is limited in its similarity to human vertebral compression fractures both in the development of the injury and the biomechanics of its regeneration due to the lack of axial weight bearing and micromotion in rodents.

Several sessions of i.v. cell administration in combination with a few weeks of PTH therapy led to remarkable regeneration of vertebral defects in rodent (**Figures 3** and **4**) and large animal porcine (**Figures 6** and **7**) models. The rodent model enabled us to test our hypothesis in osteoporotic animals, in which the healing of bone defects is severely impaired. Since the combined therapy successfully overcame this obstacle, we believe that a similar therapy in patients with osteoporosis could prove successful as well. Furthermore, using immunocompromised animals, we could specifically test the migration and differentiation of human MSCs. Others have shown that systemically administered MSCs were found in rodent fracture sites as much as 3 weeks after administration.[1–3] Therefore, we believe it would be reasonable to assume some cells survived and proliferated at the fracture site after the last injection on day 21 up to the last BLI on day 56.

Here we used minipigs, exploiting the similarity between the size of their skeletons and those of humans. Although all of the pigs were healthy, animals in the control groups did not regenerate defects within 5 weeks (**Figures 6** and **7**). Additionally, the MSCs utilized in the pig study were allogeneic and were injected without any immunosuppression therapy, since MSCs are known for their immune-privileged[37] and immunomodulatory[38] properties. The results of this study reinforce accumulating evidence that allogeneic MSCs can be used systemically without immunosuppression therapy; this has an advantage for future therapy in human clinical practice.

Surprisingly, most of the bone formed in the rat vertebral defects was found during the first 2–4 weeks postoperatively, as evident from the results of the bone volume quantification tests (**Figure 3b**), whereas the effect of the treatment on mineral density was mostly evident in the long term (**Figure 3c**).

The contribution of MSCs to the regeneration of vertebral defects was evident. It is difficult to estimate what fraction of cells administered actually migrated to the site of interest, but both *in vivo* imaging and IHF analysis detected significant populations of cells residing in the defect and nearby.

Co-localization of the DiI-stained cells and osteogenic markers showed that donor cells are not synchronized in their differentiation: some cells expressed one of the markers; some cells expressed both markers; and some did not express any at all. This finding is probably due the fact that the administered cells migrated to the site of the defect at different stages in the therapy and thus were in different stages of differentiation.

Previous studies investigated the use of small molecules to enhance migration and targeting to bone on the part of i.v.-injected MSCs.[39,40] However, in those studies, researchers did not investigate the capacity of MSCs to induce bone regeneration in an injury model but rather their ability to augment intact bone structures. Here, we showed that PTH had a significant effect on migration of MSCs to vertebral bone defects. The migration mechanism that can be enhanced by PTH has not been fully described yet; however, several of its components have been investigated and confirmed. Our results of bioluminescent imaging suggest that PTH increases migration of host MSCs to the injury site possibly via multiple pathways in addition to PTH's well-established osteoanabolic effect. The main difference between our findings and those of previous reports is that we found that PTH plays an adjuvant role in stem cell therapy and can be given at a minimal dosage for the minimal period of time required to support the migration and differentiation of multiple systemic cell injections. Our results show that hMSCs migrated to the injured vertebrae and differentiated into osteoblasts. Interestingly, hMSCs migrated to the defect site in a dose-dependent manner in response to PTH administration. However, the therapeutic effect of the dosage that induced significantly higher migration of MSCs (4 μg/kg) was not significantly different from the lower dosage (0.4 μg/kg). While we could not directly measure cell migration in pigs, we did find that when pigs were given PTH, no MSCs were found in the spleen or liver (**Supplementary Figure S2**), suggesting that PTH decreases off-target biodistribution and increases MSC migration to injury sites.

The limitations of this study include the use of a vertebral bone void model in rodents and pigs in order to simulate OVCFs. Obviously, a compressed vertebra differs greatly from a vertebra with a cylindrical defect. Yet, better animal models have not been established yet, and therefore, we have followed published studies where rats, dogs, and sheep have been used.[2,8,9,34,35,41–44] In addition, undoubtedly there is a need to verify our results in an osteoporotic large animal model. Very few attempts have been made to generate osteoporotic pigs, and so far, these have not been quite established and are extremely costly. More extended studies in pigs should be

performed in order to prove that PTH does not have toxic effects. In addition, in order to further support the hypothesis that PTH enhances the migration of injected MSCs to bone injury sites, more quantitative data is required, which could be obtained by sensitive invasive methods such as flow cytometry and PCR.

This study provides evidence for future therapies that could be attractive for the treatment of vertebral and other fragility fractures, in patients with osteoporosis. The advantage of allogeneic cells is that they do not require the patient to undergo an additional medical procedure such as bone marrow aspiration. The systemic approach holds an additional monumental advantage, making noninvasive treatment of multiple fractures at the same time without the need for surgical intervention.

MATERIALS AND METHODS

Study design. The Cedars-Sinai IACUC approved all procedures described in this study. We first tested our hypothesis in an osteoporotic immunocompromised rat model and later in a minipig model (**Figure 1a,b**). In the rat model, hMSCs were injected systemically in combination with either ldPTH or hdPTH. The extent of hMSC migration to vertebral injury sites and the possible mechanisms for this activity were evaluated using optical imaging and immunofluorescence. Bone regeneration was quantified by using *in vivo* μCT in the rat model and by using *in vivo* x-ray and *ex vivo* μCT images in the minipig model; regeneration was validated by performing histological analyses. The biodistribution of MSCs in other organs and the possible systemic effects of the treatment were evaluated as well.

Culturing of MSCs and labeling with reporter genes. Fresh human bone marrow was purchased from Lonza (Walkersville, MD), and hMSCs were isolated according to a standard procedure.[45] Briefly, bone marrow mononuclear cells were collected and plated at a density of 2×10^5 cells/cm^2. The pMSCs were isolated from porcine adipose tissue as previously reported.[46] Briefly, subcutaneous adipose tissue was harvested from euthanized minipigs, following which mononuclear cells were retrieved using enzymatic digestion and then plated at a density of 10^6 cells/cm^2. The media used for both cell types were changed two times per week.

Human MSCs were transduced with a lentiviral vector[47] harboring *Luc2* under the constitutive ubiquitin promoter, whereas pMSCs were transduced with a lentiviral vector harboring green fluorescent protein and firefly *luciferase (Luc)* under the ubiquitin promoter. Plasmids were generously provided by Dr Joseph Wu (Stanford University, Stanford, CA) and Dr Eduardo Marbán (Cedars-Sinai Medical Center, Los Angeles, CA). Both vectors were produced in 293HEK cells[47,48] before their transduction.[36] Green fluorescent protein expression was verified using flow cytometry and *Luc* expression was demonstrated using *in vitro* BLI[36] (Xenogen IVIS Spectrum; PerkinElmer, Waltham, MA). For microscopic cell identification, the cells were labeled with Vibrant-CM-DiI (Invitrogen, Life Technologies, Grand Island, NY), as previously described,[49] immediately before injection.

Vertebral defect models. The Institutional Animal Care and Use Committee of Cedars-Sinai Medical Center approved all animal procedures used in this study. Multiple vertebral defects were created in lumbar spines of osteoporotic rats and healthy minipigs. A brief description of these procedures follows, and a detailed description can be found in the **Supplementary Materials and Methods**.

Rats. Six-week-old female athymic rats (Hsd:RH-Foxn1^{rnu}), whose ovaries had been surgically removed, were purchased from Harlan Laboratories (Indianapolis, IN). Upon arrival, the rats were placed on a LCD consisting of 0.01% calcium and 0.77% phosphate (Newco Distributors, Rancho Cucamonga, CA). After 4 months of LCD, the surgical procedure was performed, and from that point onward, the rats were provided a regular diet *ad libitum*. Only data shown in **Supplementary Figure S1** was obtained in rats in which the LCD was maintained for 8 months; these animals were the exception.

Preoperatively, each rat was anesthetized by administration of 2–3% isoflurane (Piramal, Bethlehem, PA) and placed in dorsal recumbent position on a 37 °C heating pad. The skin over the L4–5 vertebrae was cleaned, clipped free of hair, and swabbed three times with solutions of Betadine and 0.5% chlorhexidine gluconate. Prior to surgery, the animal received s.c. injection of carprofen (Zoetis, Florham Park, NJ) (5 mg/kg). Following anesthetization, a sterilized surgical scalpel was used to create a 5-cm incision in the skin of each rat, and sterile soaked gauzes were used to wrap the internal organs. Next, L4 and L5 vertebral bodies were exposed. A micromotor drill (Stoelting, IL) with a 1.8-mm-diameter sterile trephine drill bit was used to create a 2.5-mm-deep bone defect through the center of the vertebral body. The s.c. tissue layer was sutured in a continuouspattern using an absorbable Vicryl 3-0 Braided (Ethicon), and the skin was sutured in a subcuticular pattern using a nonabsorbable Ethilon 2-0 Monofilament. Finally, the skin area was cleansed with sterile gauzes and a solution of 0.5% chlorhexidine gluconate.

Pigs. A total of 12 adult female Yucatan minipigs (S&S Farms) were used. The mean weight ± SD of the animals was 45.0 ± 3.6 kg and the mean age ± was 9.2 ± 1.2 months. Following an 18-hour preoperative fast, each pig was sedated with i.m. drugs (acepromazine 0.25 mg/kg (Vetone, Boise, ID), ketamine 20 mg/kg, and atropine 0.02–0.05 mg/kg (Vetone), following which the animal was injected i.v. with propofol (Fresenius Kabi, Lake Zurich, IL) (2 mg/kg) to induce full anesthesia. After this had been achieved, the trachea was intubated, and anesthesia was maintained using 1–3.5% isoflurane inhaled via the tracheal tube for the duration of the procedure. A 20-cm posterolateral skin incision was made over the lumber region (L2–5), which was then exposed by a lateral transpsoas retroperitoneal approach. In each vertebra, a critical-size cylindrical bone defect, 15-mm in depth and 4-mm in diameter, was created. After surgery, the subcutaneous tissue was closed with an absorbable subcutaneous suture and the skin with an absorbable subcuticular suture. The animal received perioperative antimicrobial prophylaxis and postoperative analgesia.

Systemic treatment with MSCs and PTH. Beginning on postoperative day 3, the rats were given PTH[26] or PBS administered s.c. daily for 3 weeks. Two different dosages of teriparatide (Eli Lilly, Indianapolis, IN)—0.4 μg/kg/day (ldPTH) or 4 μg/kg/day (hdPTH)—were used. The pigs were administered research-grade PTH (1.75 μg/kg/day) resuspended in 0.9% NaCl (adjusted to pH5) and heat-inactivated (56 °C, 1 hour) 2% pig serum (Sigma-Aldrich) or drug vehicle for 4 weeks beginning on postoperative day 5. The hMSC-Luc2 were prepared for injection and for the purposes of cell detection, injected cells were labeled with Vibrant-CM-DiI (Invitrogen) in accordance with previously described protocols.[50] Rats receiving systemic MSCs treatment were anesthetized by inhalation of 2–3% isoflurane and injected i.v. with hMSCs-Luc2 via the tail vein.[51] Each rat received a total of five injections: 2×10^6 cells per injection, every 3–4 days beginning on postoperative day 3. Similarly to hMSCs, porcine MSC-Luc was labeled with Vibrant-CM-DiI prior to the injection. Pigs receiving systemic MSCs treatment were injected i.v. with pMSCs-Luc. Each pig received a total of four injections beginning on postoperative day 5 and thereafter once a week. For each injection, 50×10^6 cells were suspended in 5 ml sterile saline and injected via the ear vein and flushed with additional 5 ml saline.

***Imaging of MSCs as they migrate to the vertebral defect site* in vivo.** Luciferase expression in the defect site was quantified using a BLI system, as described previously.[36,52] Briefly, before light detection, the rats were anesthetized by continuous administration of 1–3% isoflurane mixed with 100% oxygen. Ten minutes before imaging the rats were given an i.p. injection of 126 mg/kg luciferin (Promega, Madison, WI) in PBS. Light

emission was evaluated using the IVIS Spectrum. The exposure time was set automatically, and the bioluminescence was quantified as the total signal normalized to the exposure time and area of the region of interest.

μCT analysis of intact and operated vertebrae

In vivo μCT analysis. Vertebrae were evaluated using a cone-beam *in vivo* μCT imaging system (vivaCT 40; Scanco Medical, Brüttisellen, Switzerland). Microtomographic slices were acquired using an x-ray tube with a 55-kVp potential and reconstructed at a voxel size of 35 μm.

Assessment of vertebral defect repair. Histomorphometric 3D evaluation was performed on a volume of interest (VOI) including the trabecular region of the whole vertebra. A constrained 3D Gaussian filter ($\sigma = 0.8$, support = 1) was used to partly suppress VOI noise. The trabecular bone tissue was segmented from marrow and soft tissue by using a global thresholding procedure. A quantitative assessment of BVD and AD based on microtomographic data sets was created using direct 3D morphometry.

Rats. To analyze healing, the animals were imaged on day 1 and again 2, 4, 8, and 12 weeks after generation of the defect. Defect margins were located on day 1 scans and aligned to a standard position,[53] and a cylindrical VOI (1.68 mm in diameter, 2.52 mm in height) was defined for 3D histomorphometric evaluation. Subsequent μCT scans (those obtained at postoperative weeks 2, 4, 8, and 12) obtained in each rat were automatically registered to the standard position defined for the corresponding day 1 scan with the aid of Analyze imaging software (AnalyzeDirect, KS). The anatomical match obtained by the registration procedure allowed us to apply the exact predefined VOI of day 1 to all remaining time points. BVD and AD of the VOI were used to assess new bone formation.

Pigs. To analyze healing, x-ray films were obtained 1 week and 5 weeks after surgery. The pigs were sedated by i.m. administration of ketamine (10 mg/kg) and dexmedetomidine (0.08 mg/kg). Fluoroscopic images were acquired using the INFX-8000F DP-I system (Toshiba, Japan). Animals were placed in lateral recumbent position, and rotational acquisition was performed. The pigs were monitored during recovery from anesthesia. Immediately after the second sets of images had been obtained, the pigs were euthanized and their vertebrae excised. The vertebrae were scanned with μCT and evaluated in a previously described manner.[53] Each defect was aligned to a standard position, and a cylindrical VOI (4×15mm) was defined for 3D histomorphometric evaluation. Both the BVD and AD of the VOIs were used to assess new bone formation.

Histological analysis and immunofluorescence imaging. Histological analysis was performed on rat vertebrae that had been retrieved 12 weeks postoperatively (at the endpoint of the experiment) and on pig vertebrae that had been retrieved after 5 weeks. The vertebrae were sectioned and stained using hematoxylin and eosin for morphological analysis, as previously described.[54] For immunofluorescent staining, tissues were deparaffinized, and the antigens were retrieved by incubation in preheated Target Retrieval Solution (Dako, Carpinteria, CA) for 45 minutes in 37 °C. Nonspecific antigens were blocked by applying blocking serum–free solution (Dako). Slides were stained with primary antibodies against human bone sialoprotein and osteocalcin to examine osteogenic differentiation and with SDF1, CXCR4, EGFR, and amphiregulin to determine the MSC migration mechanism. The primary antibodies were applied to the slides and incubated in 4 °C overnight, washed off using PBS, and the slides were incubated with secondary antibodies (**Supplementary Table S1**) for 1 hour in room temperature, after which they were washed off (**Supplementary Table S1**) with PBS. Slides were then stained with 4',6-diamidino-2-phenylindole dihydrochloride (1 μg/ml) for 5minutes in the dark, after which they were again washed three times with PBS. A VectaMount mounting medium (Vector Laboratories, Burlingame, CA) was applied to the tissue. The slides were imaged using a four-channel Laser Scanning Microscope 780 (Zeiss, Pleasanton, CA) with ×20 magnification, z-stacking, and 5×5 tile scanning. For zoom-in images, a single z-stacked image was generated. All samples were scanned using the same gain and exposure settings.

Statistical analysis. GraphPad Prism 5.0b software (GraphPad Prism, San Diego, CA) was used to analyze the data. Results are presented as means ± SE (*$P \le 0.05$; **$P \le 0.01$; ***$P \le 0.001$; ****$P \le 0.0001$; ns, not significant). Longitudinal data analysis was conducted using a one-way ANOVA or two-way ANOVA with repeated measures and the Bonferroni post-test. To assess significance, $P < 0.05$ was considered statistically significant.

SUPPLEMENTARY MATERIAL

Figure S1. Establishment of the osteoporosis induction protocol in ovariectomized nude rats.

Figure S2. MSCs-hdPTH therapy regenerates vertebral defects in osteoporotic rats: histological and immunofluorescence analysis.

Figure S3. Biodistribution of cells following systemic administration.

Figure S4. Results of the metabolic toxicity study for MSC and PTH therapy.

Table S1. Antibodies used for the immunofluorescence throughout the study.

Materials and Methods

ACKNOWLEDGMENTS

The research was supported by grants from CIRM TR2-01780 and NIH (R01DE019902 and P50 AR054041). The teriparatide was a gift from Eli Lilly, Inc., Indianapolis, IN. D.S., G.S., W.T., E.M.S., Z.G., G.P., and D.G. contributed to the study concepts. W.T., D.S.J., and Y.K. performed small animal surgical procedures. W.T., D.S.J., Y.K., P.A., and H.M.B. performed large-animal experiments. X.D., G.S., M.B., E.Y., E.Z., and T.S. performed μCT imaging and data analysis. S.B.D., S.S., and D.S. were responsible for vector production, tissue staining, PCR, and microscopy. D.S., G.S., E.M.S. and G.P. wrote the manuscript. A provisional patent, assigned to Cedars-Sinai Medical Center and Rochester University, is pending. The authors declare no other competing financial interests.

REFERENCES

1. National Osteoporosis Foundation (2013). *Debunking the Myths*. http://nof.org/articles/4.
2. Wang, ML, Massie, J, Perry, A, Garfin, SR and Kim, CW (2007). A rat osteoporotic spine model for the evaluation of bioresorbable bone cements. *Spine J* **7**: 466–474.
3. Sandhu, SK and Hampson, G (2011). The pathogenesis, diagnosis, investigation and management of osteoporosis. *J Clin Pathol* **64**: 1042–1050.
4. Chamberlain, G, Fox, J, Ashton, B and Middleton, J (2007). Concise review: mesenchymal stem cells: their phenotype, differentiation capacity, immunological features, and potential for homing. *Stem Cells* **25**: 2739–2749.
5. Center, JR, Nguyen, TV, Schneider, D, Sambrook, PN and Eisman, JA (1999). Mortality after all major types of osteoporotic fracture in men and women: an observational study. *Lancet* **353**: 878–882.
6. Brack, AS and Rando, TA (2007). Intrinsic changes and extrinsic influences of myogenic stem cell function during aging. *Stem Cell Rev* **3**: 226–237.
7. Sethe, S, Scutt, A and Stolzing, A (2006). Aging of mesenchymal stem cells. *Ageing Res Rev* **5**: 91–116.
8. Turner, TM, Urban, RM, Singh, K, Hall, DJ, Renner, SM, Lim, TH *et al.* (2008). Vertebroplasty comparing injectable calcium phosphate cement compared with polymethylmethacrylate in a unique canine vertebral body large defect model. *Spine J* **8**: 482–487.
9. Verron, E, Pissonnier, ML, Lesoeur, J, Schnitzler, V, Fellah, BH, Pascal-Moussellard, H *et al.* (2014). Vertebroplasty using bisphosphonate-loaded calcium phosphate cement in a standardized vertebral body bone defect in an osteoporotic sheep model. *Acta Biomater* **10**: 4887–4895.
10. Bruder, SP, Fink, DJ and Caplan, AI (1994). Mesenchymal stem cells in bone development, bone repair, and skeletal regeneration therapy. *J Cell Biochem* **56**: 283–294.
11. Dennis, JE, Merriam, A, Awadallah, A, Yoo, JU, Johnstone, B and Caplan, AI (1999). A quadripotential mesenchymal progenitor cell isolated from the marrow of an adult mouse. *J Bone Miner Res* **14**: 700–709.
12. Kaback, LA, Soung, do Y, Naik, A, Geneau, G, Schwarz, EM, Rosier, RN *et al.* (2008). Teriparatide (1-34 human PTH) regulation of osterix during fracture repair. *J Cell Biochem* **105**: 219–226.
13. Yu, B, Zhao, X, Yang, C, Crane, J, Xian, L, Lu, W *et al.* (2012). Parathyroid hormone induces differentiation of mesenchymal stromal/stem cells by enhancing bone morphogenetic protein signaling. *J Bone Miner Res* **27**: 2001–2014.
14. Carpio, L, Gladu, J, Goltzman, D and Rabbani, SA (2001). Induction of osteoblast differentiation indexes by PTHrP in MG-63 cells involves multiple signaling pathways. *Am J Physiol Endocrinol Metab* **281**: E489–E499.
15. Jung, Y, Wang, J, Schneider, A, Sun, YX, Koh-Paige, AJ, Osman, NI *et al.* (2006). Regulation of SDF-1 (CXCL12) production by osteoblasts; a possible mechanism for stem cell homing. *Bone* **38**: 497–508.

16. Huber, BC, Brunner, S, Segeth, A, Nathan, P, Fischer, R, Zaruba, MM *et al.* (2011). Parathyroid hormone is a DPP-IV inhibitor and increases SDF-1-driven homing of CXCR4(+) stem cells into the ischaemic heart. *Cardiovasc Res* **90**: 529–537.
17. Zhu, J, Siclari, VA, Liu, F, Spatz, JM, Chandra, A, Divieti Pajevic, P *et al.* (2012). Amphiregulin-EGFR signaling mediates the migration of bone marrow mesenchymal progenitors toward PTH-stimulated osteoblasts and osteocytes. *PLoS One* **7**: e50099.
18. Greenspan, SL, Bone, HG, Ettinger, MP, Hanley, DA, Lindsay, R, Zanchetta, JR *et al.*; Treatment of Osteoporosis with Parathyroid Hormone Study Group. (2007). Effect of recombinant human parathyroid hormone (1-84) on vertebral fracture and bone mineral density in postmenopausal women with osteoporosis: a randomized trial. *Ann Intern Med* **146**: 326–339.
19. Alkhiary, YM, Gerstenfeld, LC, Krall, E, Westmore, M, Sato, M, Mitlak, BH *et al.* (2005). Enhancement of experimental fracture-healing by systemic administration of recombinant human parathyroid hormone (PTH 1-34). *J Bone Joint Surg Am* **87**: 731–741.
20. Aspenberg, P, Genant, HK, Johansson, T, Nino, AJ, See, K, Krohn, K *et al.* (2010). Teriparatide for acceleration of fracture repair in humans: a prospective, randomized, double-blind study of 102 postmenopausal women with distal radial fractures. *J Bone Miner Res* **25**: 404–414.
21. Peichl, P, Holzer, LA, Maier, R and Holzer, G (2011). Parathyroid hormone 1-84 accelerates fracture-healing in pubic bones of elderly osteoporotic women. *J Bone Joint Surg Am* **93**: 1583–1587.
22. Song, J, Jin, Z, Chang, F, Li, L and Su, Y (2014). Single and combined use of human parathyroid hormone (PTH) (1-34) on areal bone mineral density (aBMD) in postmenopausal women with osteoporosis: evidence based on 9 RCTs. *Med Sci Monit* **20**: 2624–2632.
23. Grosso, MJ, Courtland, HW, Yang, X, Sutherland, JP, Stoner, K, Nguyen, J *et al.* (2015). Intermittent PTH administration and mechanical loading are anabolic for periprosthetic cancellous bone. *J Orthop Res* **33**: 163–173.
24. Chen, P, Miller, PD, Recker, R, Resch, H, Rana, A, Pavo, I *et al.* (2007). Increases in BMD correlate with improvements in bone microarchitecture with teriparatide treatment in postmenopausal women with osteoporosis. *J Bone Miner Res* **22**: 1173–1180.
25. Lindsay, R, Zhou, H, Cosman, F, Nieves, J, Dempster, DW and Hodsman, AB (2007). Effects of a one-month treatment with PTH(1-34) on bone formation on cancellous, endocortical, and periosteal surfaces of the human ilium. *J Bone Miner Res* **22**: 495–502.
26. Dhillon, RS, Xie, C, Tyler, W, Calvi, LM, Awad, HA, Zuscik, MJ *et al.* (2013). PTH-enhanced structural allograft healing is associated with decreased angiopoietin-2-mediated arteriogenesis, mast cell accumulation, and fibrosis. *J Bone Miner Res* **28**: 586–597.
27. Komatsu, DE, Brune, KA, Liu, H, Schmidt, AL, Han, B, Zeng, QQ *et al.* (2009). Longitudinal *in vivo* analysis of the region-specific efficacy of parathyroid hormone in a rat cortical defect model. *Endocrinology* **150**: 1570–1579.
28. Manabe, T, Mori, S, Mashiba, T, Kaji, Y, Iwata, K, Komatsubara, S *et al.* (2007). Human parathyroid hormone (1-34) accelerates natural fracture healing process in the femoral osteotomy model of cynomolgus monkeys. *Bone* **40**: 1475–1482.
29. Daugaard, H, Elmengaard, B, Andreassen, TT, Lamberg, A, Bechtold, JE and Soballe, K (2012). Systemic intermittent parathyroid hormone treatment improves osseointegration of press-fit inserted implants in cancellous bone. *Acta Orthop* **83**: 411–419.
30. Neer, RM, Arnaud, CD, Zanchetta, JR, Prince, R, Gaich, GA, Reginster, JY *et al.* (2001). Effect of parathyroid hormone (1-34) on fractures and bone mineral density in postmenopausal women with osteoporosis. *N Engl J Med* **344**: 1434–1441.
31. Phillips, FM, Turner, AS, Seim, HB 3rd, MacLeay, J, Toth, CA, Pierce, AR *et al.* (2006). *In vivo* BMP-7 (OP-1) enhancement of osteoporotic vertebral bodies in an ovine model. *Spine J* **6**: 500–506.
32. Govindarajan, P, Böcker, W, El Khassawna, T, Kampschulte, M, Schlewitz, G, Huerter, B *et al.* (2014). Bone matrix, cellularity, and structural changes in a rat model with high-turnover osteoporosis induced by combined ovariectomy and a multiple-deficient diet. *Am J Pathol* **184**: 765–777.
33. Gao, X, Ma, W, Dong, H, Yong, Z and Su, R (2014). Establishing a rapid animal model of osteoporosis with ovariectomy plus low calcium diet in rats. *Int J Clin Exp Pathol* **7**: 5123–5128.
34. Liang, H, Wang, K, Shimer, AL, Li, X, Balian, G and Shen, FH (2010). Use of a bioactive scaffold for the repair of bone defects in a novel reproducible vertebral body defect model. *Bone* **47**: 197–204.
35. Liang, H, Li, X, Shimer, AL, Balian, G and Shen, FH (2014). A novel strategy of spine defect repair with a degradable bioactive scaffold preloaded with adipose-derived stromal cells. *Spine J* **14**: 445–454.
36. Sheyn, D, Kallai, I, Tawackoli, W, Cohn Yakubovich, D, Oh, A, Su, S *et al.* (2011). Gene-modified adult stem cells regenerate vertebral bone defect in a rat model. *Mol Pharm* **8**: 1592–1601.
37. De Miguel, MP, Fuentes-Julián, S, Blázquez-Martínez, A, Pascual, CY, Aller, MA, Arias, J *et al.* (2012). Immunosuppressive properties of mesenchymal stem cells: advances and applications. *Curr Mol Med* **12**: 574–591.
38. Dazzi, F, Lopes, L and Weng, L (2012). Mesenchymal stromal cells: a key player in 'innate tolerance'? *Immunology* **137**: 206–213.
39. Yao, W, Guan, M, Jia, J, Dai, W, Lay, YA, Amugongo, S *et al.* (2013). Reversing bone loss by directing mesenchymal stem cells to bone. *Stem Cells* **31**: 2003–2014.
40. Guan, M, Yao, W, Liu, R, Lam, KS, Nolta, J, Jia, J *et al.* (2012). Directing mesenchymal stem cells to bone to augment bone formation and increase bone mass. *Nat Med* **18**: 456–462.
41. Zhu, X, Chen, X, Chen, C, Wang, G, Gu, Y, Geng, D *et al.* (2012). Evaluation of calcium phosphate and calcium sulfate as injectable bone cements in sheep vertebrae. *J Spinal Disord Tech* **25**: 333–337.
42. Zhu, XS, Zhang, ZM, Mao, HQ, Geng, DC, Zou, J, Wang, GL *et al.* (2011). A novel sheep vertebral bone defect model for injectable bioactive vertebral augmentation materials. *J Mater Sci Mater Med* **22**: 159–164.
43. Yang, HL, Zhu, XS, Chen, L, Chen, CM, Mangham, DC, Coulton, LA *et al.* (2012). Bone healing response to a synthetic calcium sulfate/β-tricalcium phosphate graft material in a sheep vertebral body defect model. *J Biomed Mater Res B Appl Biomater* **100**: 1911–1921.
44. Vaněček, V, Klíma, K, Kohout, A, Foltán, R, Jiroušek, O, Šedý, J *et al.* (2013). The combination of mesenchymal stem cells and a bone scaffold in the treatment of vertebral body defects. *Eur Spine J* **22**: 2777–2786.
45. Aslan, H, Zilberman, Y, Arbeli, V, Sheyn, D, Matan, Y, Liebergall, M *et al.* (2006). Nucleofection-based *ex vivo* nonviral gene delivery to human stem cells as a platform for tissue regeneration. *Tissue Eng* **12**: 877–889.
46. Dubois, SG, Floyd, EZ, Zvonic, S, Kilroy, G, Wu, X, Carling, S *et al.* (2008). Isolation of human adipose-derived stem cells from biopsies and liposuction specimens. *Methods Mol Biol* **449**: 69–79.
47. Li, Z, Suzuki, Y, Huang, M, Cao, F, Xie, X, Connolly, AJ *et al.* (2008). Comparison of reporter gene and iron particle labeling for tracking fate of human embryonic stem cells and differentiated endothelial cells in living subjects. *Stem Cells* **26**: 864–873.
48. Sun, N, Lee, A and Wu, JC (2009). Long term non-invasive imaging of embryonic stem cells using reporter genes. *Nat Protoc* **4**: 1192–1201.
49. Sheyn, D, Kimelman-Bleich, N, Pelled, G, Zilberman, Y, Gazit, D and Gazit, Z (2008). Ultrasound-based nonviral gene delivery induces bone formation in vivo. *Gene Ther* **15**: 257–266.
50. Kallmes, DF, Comstock, BA, Heagerty, PJ, Turner, JA, Wilson, DJ, Diamond, TH *et al.* (2009). A randomized trial of vertebroplasty for osteoporotic spinal fractures. *N Engl J Med* **361**: 569–579.
51. Weaver, AS, Su, YP, Begun, DL, Miller, JD, Alford, AI and Goldstein, SA (2010). The effects of axial displacement on fracture callus morphology and MSC homing depend on the timing of application. *Bone* **47**: 41–48.
52. Kimelman-Bleich, N, Pelled, G, Zilberman, Y, Kallai, I, Mizrahi, O, Tawackoli, W *et al.* (2011). Targeted gene-and-host progenitor cell therapy for nonunion bone fracture repair. *Mol Ther* **19**: 53–59.
53. Kallai, I, Mizrahi, O, Tawackoli, W, Gazit, Z, Pelled, G and Gazit, D (2011). Microcomputed tomography-based structural analysis of various bone tissue regeneration models. *Nat Protoc* **6**: 105–110.
54. Sheyn, D, Cohn Yakubovich, D, Kallai, I, Su, S, Da, X, Pelled, G *et al.* (2013). PTH promotes allograft integration in a calvarial bone defect. *Mol Pharm* **10**: 4462–4471.